COMMUNICATION

Detecting 100 fW cm^{-2} Light with Trapped Electron Gated Organic Phototransistors

*Yang Zhang, Yongbo Yuan, and Jinsong Huang**

Photodetectors are optoelectronic devices that convert light signals into detectable electrical signals, and they are the "electronic eye" that extends the limits of human vision in both spectral response range and lowest detectable light intensity. Photodetectors capable of sensing ultraweak light have broad applications in various fields, including quantum communication and cryptography, military, astronomy, industry, consumer electronics, etc.[1–3] Among all types of solid-state photodetectors, phototransistors are attracting a lot of interests owing to their very high responsivity that holds promise for detecting ultraweak light.[4–6] For example, Qi et al. demonstrated a high responsivity of 2.2×10^4 A W^{-1} toward ultraviolet (UV) lights with thermally stable organic phototransistors based on PSeTPTI/$PC_{61}BM$.[5] In another work, Zhao et al. proposed a UV-sensitive organic phototransistors using benzo[1,2-b:4,5-b′]dithiophene dimers as the conduction channel, where a responsivity of ≈10^4 A W^{-1} was achieved.[6] Phototransistors are a class of transistors with the possibility to modulate their channel current not only by the regular gate but also by the incident photons. These phototransistors combine the gain of transistor and regular photoconductor, which can generate a huge apparent gain. For this reason, phototransistors have been exploited for detecting ultraweak light and even single photons. For example, Gansen et al. employed δ-doped GaAs/$Al_{0.2}Ga_{0.8}As$ phototransistors for detecting single photons.[7] In their work, a layer of InGaAs quantum dots (QDs) was sandwiched between the gate and the conduction channel to form a floating gate in the transistor. Upon single photon impinging, this floating gate was charged with photogenerated holes, which resulted in a rightward shift of the transfer curve of the transistor due to the partial screening of the gate electric field by the charged QDs. However, it should be noted that the impressive performance of their phototransistors was achieved at 4 K, which is a temperature apparently too low for most of the practical applications. Moreover, the fabrication of their devices might not be cost-effective since it involved molecular beam epitaxy for the growth of QDs.

To circumvent these issues, we propose a type of room-temperature operation floating-gate phototransistors. We implement the design with organic semiconductors as conduction channel and light-absorbing layer. Organic semiconductors are promising materials for solid-state light detection due to their low cost, light weight, flexibility, low-temperature, and solution processability.[8] The fabricated phototransistors operating at off-state exhibit a very low noise current of ≈100 pA, and they have a huge apparent gain of the order of ≈10^8. The combination of high gain and low noise of the floating-gate organic phototransistors enables the detection of ultraweak light down to ≈100 fW cm^{-2}, which represents the lowest light intensity detected without using lock-in techniques by solution processed cooling-free photodetectors.

Figure 1a depicts the general design of the phototransistor. Here, we adopt a bottom-gate-top-contact geometry for the transistor. The light-absorbing layer is a blend of organic semiconductors that form bulk heterojunctions, and it acts as a light-enabled floating gate that gives rise to the transistor photoresponse, which is characterized by the change of drain–source (channel) current (ΔI_{ds}), or by the shift of threshold voltage (ΔV_{th}) on the transfer characteristics relative to their respective values in the dark, as illustrated in Figure 1b. The detailed operation principle of the device is illustrated in Figure 1c. In the dark, the device works as a regular transistor and the injection current through the top dielectric is largely suppressed by the energy barrier between the channel and the light-absorbing layer, as represented by the crosses in Figure 1c. Upon light illumination, free electrons and holes are generated in the light-absorbing bulk heterojunction layer. Directed by the vertical gate electric field, electrons drift toward the light-absorbing layer/bottom dielectric interface and get trapped there by hydroxyl groups or other functional groups,[9] while holes drift toward the top dielectric/light-absorbing layer interface and accumulate or get trapped there, as indicated by the white arrows in Figure 1c. Previous work shows that although the organic semiconductor conduction channel is p-type, electrons can be injected into the channel and accumulate near the drain electrode where there is very large applied electric field.[10] In the proposed transistors, these electrons are further constrained by photogenerated holes located at the top dielectric/light-absorbing layer interface via coulombic interaction, as indicated by the double arrow in Figure 1c. As a result of the coulombic interaction, the energy barrier between the channel and the light-absorbing layer is effectively thinned. Driven by the gate electric field and coulombic attraction, electrons travel readily through the top dielectrics and get trapped at the top dielectric/light-absorbing layer interface (Figure 1c). This light-triggered multiple electron injection process is of vital importance in enabling the proposed phototransistor for detecting ultraweak light. To facilitate this process, a current-injection top dielectric is intentionally introduced between the conduction channel and the light-absorbing layer to increase the amount of electrons that are injected into and trapped at the light-absorbing layer (floating gate) upon light illumination. We

Dr. Y. Zhang, Dr. Y. Yuan, Prof. J. Huang
Department of Mechanical and Materials Engineering
University of Nebraska–Lincoln
Lincoln, NE 68588-0656, USA
E-mail: jhuang2@unl.edu

DOI: 10.1002/adma.201603969

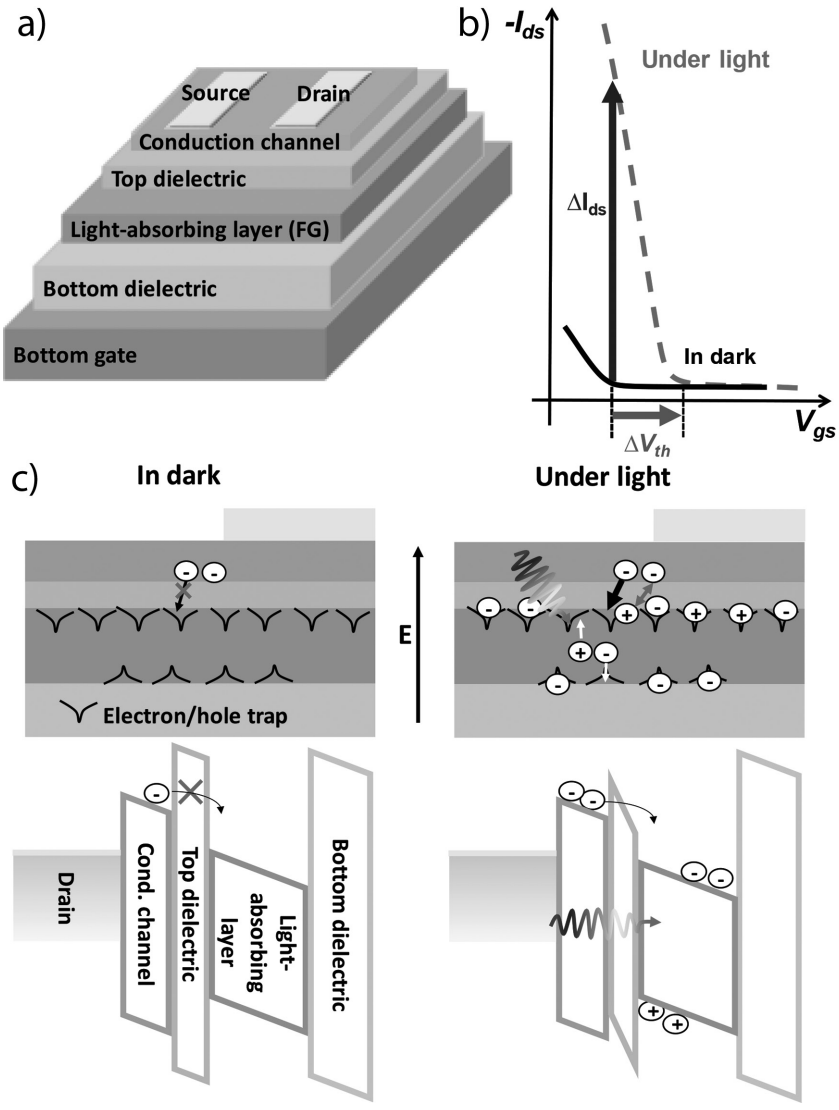

Figure 1. a) Schematic depicting the device design of current-injection enabled highly sensitive organic phototransistor. FG stands for floating gate. b) Sketch illustrating the transfer characteristics of a phototransistor in the dark and under light and the photoresponse that is represented by ΔI_{ds} (change of the drain–source current) and ΔV_{th} (change of the threshold voltage). c) Schematics illustrating the operating mechanism of the proposed phototransistor. The upper and lower panels depict device cross-sections together with interfacial electron/hole traps and the energy level diagrams of the device under different lighting conditions, respectively. Circles with minus (plus) sign represent electrons (holes). The white arrows indicate the moving of the electron/hole under electric field. The black arrows across the top dielectric denote electron injection, and the double arrow indicates the coulombic interaction between electrons and holes.

remark that the electron injection in the dark is blocked by the energy barriers and thus should not significantly affect the dark current.

With the trapped electrons as a floating gate, ΔI_{ds} can be approximated in the saturation regime by (see the Supporting Information for details)

$$\Delta I_{ds} = \frac{\mu W e^2 \sigma^2}{2LC_{tot}} \quad (1)$$

where μ is the carrier mobility, W (L) is the channel width (length), C_{tot} is the total specific capacitance of the dielectrics between the gate and the conduction channel, e is the elementary charge, and σ is the density of trapped electrons that form a floating gate in Figure 1a. As revealed by Equation (1), the change of drain–source current ΔI_{ds} increases quadratically with the trapped electron density σ. Furthermore, one can assume a stretched exponential-like relationship between the trapped electron density (σ) caused by electron injection and the number of incident (absorbed) photons per area per certain period (Φ) for the light-triggered multiple electron injection mechanism, and Equation (1) can then be expressed as

$$\Delta I_{ds} = A\frac{\mu W e^2}{2LC_{tot}}\exp\left(B\Phi^n\right) \quad (2)$$

where A, B, and n are constants. Equation (2) indicates that the incident photons can spark an exponential change in the channel current. In other words, the light signal is amplified by the multiple electron injection process following an exponential relationship. This amplification effect combined with a low noise current by biasing the device to an off-state, give rise to an ultrahigh sensitivity in the phototransistor shown in Figure 1a.

To implement the device design in Figure 1a, we fabricated phototransistors with a material structure shown in **Figure 2**a. The highly p-doped silicon substrate was used as the bottom gate, while 60 nm silver was thermally evaporated on the top using a shadow mask to serve as source and drain contacts which define a channel length of 100 μm and a width of 1 mm. A bulk heterojunction layer formed by a blend of 2,6-bis(trimethyltin)-4,8-bis(5-(2-ethylhexyl)-thiophen-2-yl)benzo[1,2-b:4,5-b′]dithiophene (PBDTTT):[6,6]-phenyl C61 butyric acid methyl ester (PCBM), which has been demonstrated in achieving highly efficient organic solar cells,[11] was chosen as the floating gate. The PBDTTT:PCBM blending layer was deposited on the Si substrate coated with 300 nm thick dry thermal oxide (bottom dielectric) to function as the UV–visible light-absorbing layer of the phototransistor.

The top dielectrics consisted of a stack of a cross-linked poly(4-vinylphenol) (PVP) layer and a lithium fluoride (LiF) layer. The PVP layer cross-linked with 4,4′-(hexafluoroisopropylidene)diphthalic anhydride (HDA) was spin-coated directly on top of the PBDTTT:PCBM layer. In order to provide adequate surface wettability for the subsequent spin-coating of C8-BTBT in 1,2-dichlorobenzene (DCB), a 20 nm thick LiF layer was deposited on the cross-linked PVP:HDA layer by

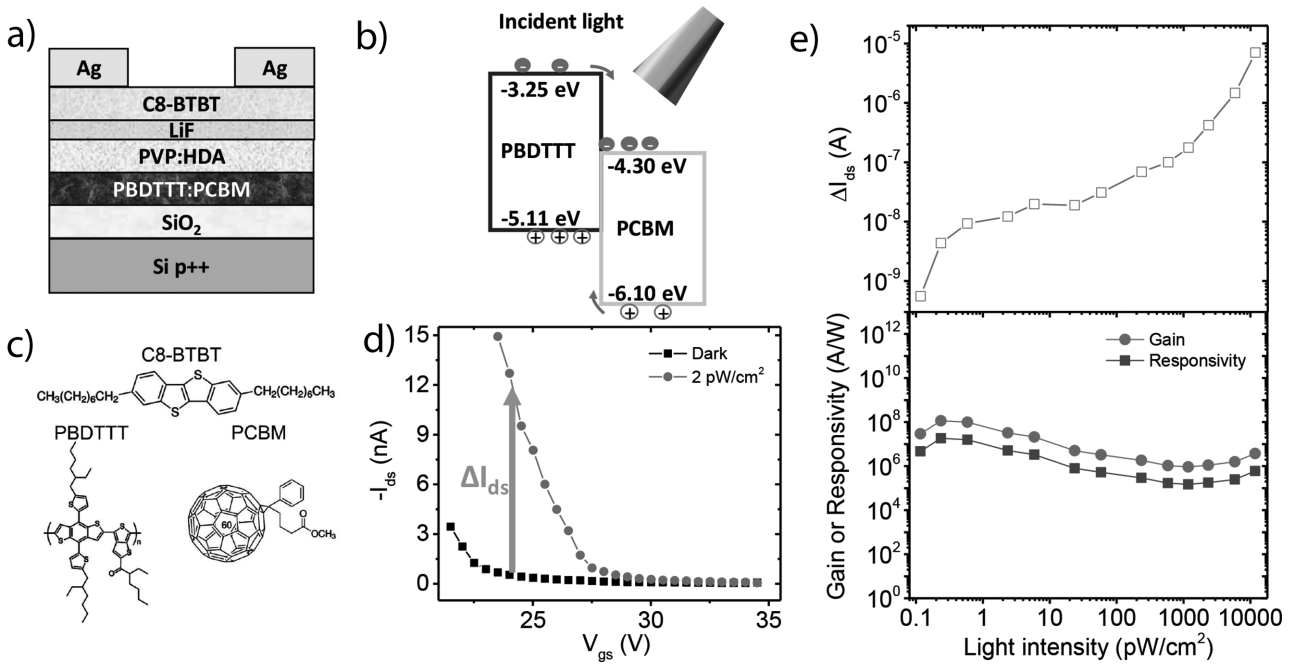

Figure 2. a) Schematic illustrating the material structure of the implemented phototransistors. b) Energy level diagram formed by the PBDTTT:PCBM bulk heterojunction, along with the illustration of the photocarrier generation and separation process. The numbers with minus sign indicate the positions of highest occupied molecular orbital (HOMO) and lowest unoccupied molecular orbital (LUMO) levels relative to the vacuum level. c) Molecular structures of C8-BTBT, PBDTTT, and PCBM. d) Representative transfer characteristics recorded in the dark (square) and under ≈2 pW cm^{-2} red light (circle) for the phototransistor shown in (a). I_{ds} is the drain–source current, and V_{gs} is the applied bias between gate and source. The drain–source voltage bias V_{ds} was fixed at −40 V. The arrow indicates the change of the drain–source current caused by the incident light. e) Photoresponse ΔI_{ds} (upper panel) and gain/responsivity (lower panel) of the phototransistor under various light intensities. These data were extracted from Figure S1 (Supporting Information) at V_{gs} = 24 V.

thermal evaporation. This LiF layer is transparent in the UV–visible range since it has a bandgap of 13.6 eV.[12] Eventually, the C8-BTBT conduction channel was formed by the off-center spin-coating method developed previously by us.[13] C8-BTBT film grown with this method is known to offer very high hole mobility and good stability in ambient conditions, owing to its high crystallinity resulting from the ordered assembly of C8-BTBT molecules during the spin-coating process.[13,14] Figure 2b illustrates the energy level diagram of the bulk heterojunction formed by PBDTTT and PCBM.[11,15] When UV–visible photons are absorbed by the PBDTTT:PCBM layer, free electrons and holes are generated and spatially separated by the heterojunction. Figure 2c shows the molecular structures of C8-BTBT, PBDTTT, and PCBM used in this work.

Figure 2d shows the typical transfer characteristics of the fabricated phototransistors recorded in the dark and under 2 pW cm^{-2} red light (660 nm). The 2 pW cm^{-2} light impinging on the phototransistor sparked a significant change in the drain–source current (≈10 nA). Transfer characteristics recorded under ≈100 fW cm^{-2} to ≈11 nW cm^{-2} illuminations can be found in Figure S1 (Supporting Information). The increase of I_{ds} with decreasing V_{gs} under negative drain–source bias indicates that holes are the majority carriers that conduct current in the channel, which is consistent with our previous reports.[13,14] The photoresponse of the transistor increases monotonically with light intensity (upper panel of Figure 2e), and fitting the data with Equation (2) yields an n of ≈0.2 (Figure S2, Supporting Information). This phototransistor demonstrates a ΔI_{ds} of ≈550 pA (which is more than five times larger than the off-current) at an ultraweak light intensity of ≈100 fW cm^{-2}. The high sensitivity at very low light illumination is further confirmed with the measurements in Figure S3 (Supporting Information), where the recovery of the transfer curve after removing the illumination (≈100 fW cm^{-2}) is clearly demonstrated. To the best of our knowledge, this is the lowest reported light intensity that can be directly detected without using lock-in techniques at room temperature by a solution processed photodetector. Figure S4a (Supporting Information) shows the decent reproducibility of the transfer characteristics recorded in the dark, which suggests that the electron injection in the dark is largely suppressed. We note that this stable behavior of the transistor in the dark is of paramount importance in the successful detection of ultraweak light. Figure S4b (Supporting Information) presents five cycles of transfer characteristics recorded under light, where reproducible detection of ultraweak light (≈100 fW cm^{-2}) was successfully showcased.

Responsivity and gain are important figures of merit to characterize photodetector performance. The responsivity here is defined as the change of I_{ds} per incident light power, and the gain is the number of charges collected by the electrodes per absorbed photon. In phototransistors, both responsivity and gain are proportional to ΔI_{ds} at given V_{ds} and V_{gs}. The typical responsivity and gain of the phototransistor are presented in the lower panel of Figure 2e. In general, the phototransistor maintained ultrahigh responsivities (gains) over the entire light intensity range (100 fW cm^{-2}–11 nW cm^{-2}), and demonstrated

a peak responsivity of 1.8×10^7 A W^{-1} (corresponds to a gain of 1.2×10^8) at a light intensity of ≈200 fW cm^{-2}. The gain is calculated by taking into account a 30% light absorption at 660 nm (Figure S5, Supporting Information). This responsivity (gain) is among the highest reported to date on photodetectors.[16]

Alternatively, the photoresponse of transistors can be expressed as the shift of the threshold voltage (ΔV_{th} in Figure 1b, defined by Equation (S5) in the Supporting Information). In analogy to the current responsivity shown in Figure 2e, we introduce a voltage responsivity (R_V) for phototransistors which is defined as the change of the threshold voltage (ΔV_{th}) per incident light power (**Figure 3**). In general, the voltage responsivity decreases with the light intensity, following a power law of $R_V \propto P^{-0.8}$, where P is the incident light intensity. The phototransistor registered an unprecedented voltage responsivity of 2.2×10^{16} V W^{-1} at the lowest detectable light intensity (≈100 fW cm^{-2}), which is more than ten orders of magnitude higher than that achieved on recently reported carbon nanotube-based phototransistors.[17]

From the proposed operation principle, the light-triggered multiple electron injection process plays a key role in enabling these phototransistors for detecting ultraweak light signals. To further clarify the origin of the high sensitivity, we estimate the density of the electrons trapped at the PVP:HDA/PBDTTT:PCBM interface and compare it with the photogenerated hole density. Under ≈100 fW cm^{-2} illumination, the transfer curve in Figure S1a (Supporting Information) exhibits a threshold voltage shift of 2.55 V (relative to the value in the dark), which corresponds to a trapped electron density of 1.4×10^{11} cm^{-2}, as evaluated with the following equation[18]

$$\sigma = \Delta V_{th} C_{tot} / e \tag{3}$$

On the other hand, the upper limit (by assuming 100% quantum efficiency and no recombination) of the photogenerated hole density with a light intensity of 100 fW cm^{-2} for an illumination period of 1 min is found to be 2×10^7 cm^{-2}. Comparing these two densities leads to the conclusion that at least ≈10^4 electrons are injected per absorbed photon. This result further confirms that the light-triggered multiple electron injection process serves, in effect, to amplify ultraweak light signals, which enables the demonstrated exceptionally high responsivity (gain).

To verify the existence of the light-triggered electron injection, we monitored the current between the drain and gate while turning the light of 660 nm on and off, as shown in **Figure 4**a. The gate-to-drain current ($-I_{dg}$) exhibited immediate response to the light in four consecutive on–off cycles (Figure 4b). This current flew through the SiO_2 dielectric rather than charging the SiO_2 capacitor, as the amount of charges that had passed the circuit for a period of 1 min was much larger than the maximum charges that could be stored on the capacitor. Since the C8-BTBT layer does not absorb light above ≈375 nm, the response shown in Figure 4b can only originate from the light absorption in the PBDTTT:PCBM layer, confirming

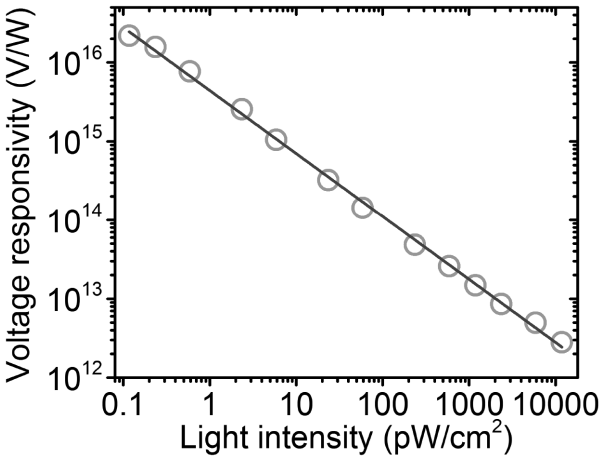

Figure 3. Voltage responsivity of the phototransistor as a function of light intensity. Threshold voltages under different light intensities were obtained from the $|I_{ds}|^{0.5}$ versus V_{gs} plots (similar to the one shown in Figure S6 in the Supporting Information), and were used for the calculation of the voltage responsivity. The line is a linear fit to the data that gives a slope of –0.8 on a log–log plot.

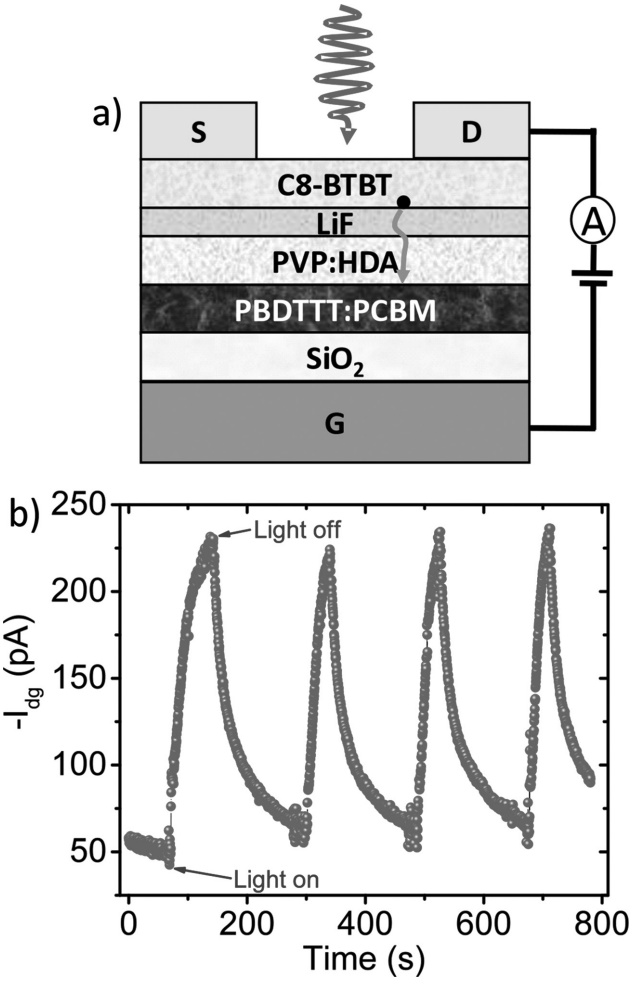

Figure 4. a) Schematic diagram showing the setup for the measurement in panel (b). The black dot and the arrow illustrate an electron that is about to travel through the top dielectrics under light illumination. b) The gate (G)-to-drain (D) current recorded over time at a V_{dg} of –40 V while turning the light (center wavelength at 660 nm with an intensity of 36.3 μW cm^{-2}) on and off for four cycles.

the existence of light-induced current flowing into the drain electrode. It is worth mentioning that we also fabricated phototransistors with a 20 nm HfO_2 layer grown by atomic layer deposition (ALD) at 100 °C (Figure S7a, Supporting Information) as the top dielectric layer. The injection current through the HfO_2 layer was more than six orders of magnitude lower than that through the PVP:HDA layer (Figures S7d and S8b, Supporting Information). Therefore, the gate-to-drain current (mainly injected electron current) should be largely suppressed, while the total specific capacitance C_{tot} was found to be 11.2 nF cm^{-2}, comparable to the capacitance (8.9 nF cm^{-2}) of the device shown in Figure 2a. The transfer characteristics of the transistor with HfO_2 as the top dielectric are displayed in Figure S7b (Supporting Information). The transistor showed negligible response (ΔI_{ds}) toward ultraweak lights, highlighting the importance of introducing the electron injection top dielectrics in achieving extremely high sensitivity in phototransistors.

Photoresponse to visible lights is highly desired when using photodetectors for radiation detections, as many widely used scintillators emit in the visible range (e.g., NaI (TI), CsI (TI), BGO, etc.) As a step forward from our previous work where the detectors' response was confined to UV lights,[14] phototransistors proposed here exhibit a broad response to light in the UV–visible range. **Figure 5** shows the typical photoresponse (ΔI_{ds}) of the phototransistors at wavelengths from 300 to 900 nm, along with the optical absorption of the PBDTTT:PCBM layer. The very good agreement between the current spectrum and the optical absorption curve further confirms that the photoresponse of the detector in the visible range indeed originates from the light absorption in the PBDTTT:PCBM layer. This result also suggests another important merit of employing light-absorbing polymer blend as a floating gate, i.e., the detecting wavelength range may be easily tailored by using different light-absorbing polymers without losing the high gain.

In summary, we proposed a general phototransistor architecture for detecting ultraweak light into the fW cm^{-2} region at room temperature. In addition, we implemented the design with organic phototransistors comprising a PBDTTT:PCBM light-absorbing layer sandwiched between the bottom gate and the conduction channel, and demonstrated room-temperature detection of ultraweak light down to ≈100 fW cm^{-2}. This exceptionally high sensitivity was brought about by an amplification process triggered by incident light. With these phototransistors, we achieved an astonishingly high responsivity of ≈10^7 A W^{-1} at a light intensity of ≈200 fW cm^{-2}. This high responsivity, together with the relatively low operating voltage, make the phototransistors promising candidates for applications where high voltage bias is unwanted.

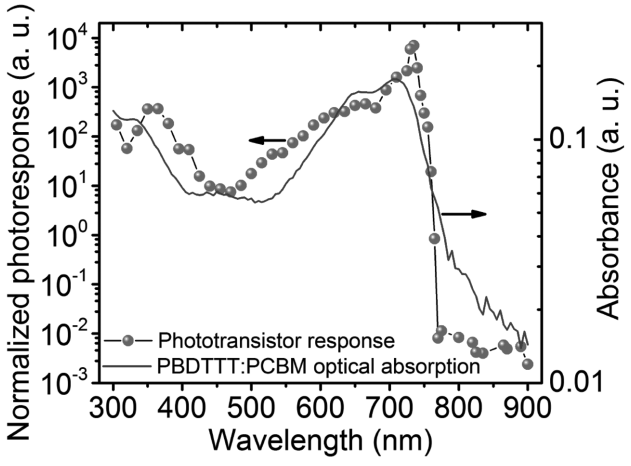

Figure 5. Spectral response (ΔI_{ds}) of the photodetector normalized with respect to the light intensity at each wavelength (circles) along with the optical absorption of the PBDTTT:PCBM layer (line).

Experimental Section

Device Fabrication: All phototransistors in this work were fabricated on highly p-doped (resistivity: 0.001–0.005 Ω cm) silicon substrates coated with a 300 nm thick dry thermal oxide layer. The PBDTTT:PCBM solution was prepared by dissolving PBDTTT:PCBM in DCB with a concentration of 10:15 mg mL^{-1} and keeping stirring the solution for at least 36 h at 50 °C. The light-absorbing layer was formed by spin-coating the PBDTTT:PCBM solution on the substrate at a speed of 2000 rpm for 60 s, which resulted in a film thickness of ≈50 nm. Before spin-coating, the PBDTTT:PCBM solution and the substrate were heated to 70 °C to achieve better uniformity for the PBDTTT:PCBM layer. The PVP:HDA solution was prepared in the same way as detailed in ref. [13], and the diluted solution was spin-coated on the PBDTTT:PCBM layer at 4000 rpm. The sample was then subjected to a thermal annealing on a hotplate at 105 °C for 1 h, and a subsequent UV-ozone treatment (UVO cleaner, Jelight Company Inc.) for 5 min. The resulting thickness of the cross-linked PVP layer was ≈45 nm. Next, a LiF layer was thermally evaporated on top of the PVP layer at a rate of ≈0.1 Å s^{-1}. The C8-BTBT conduction channel was grown by the off-center spin-coating method as described in ref. [13]. Source/drain contacts were obtained by thermal deposition of 60 nm silver through a silicon shadow mask.

Light Sensing (Transfer Characteristics) Measurement: A light-emitting diode (LED) emitting at a center wavelength of 660 nm was used as the light source to illuminate the phototransistor from the top. The light intensity reaching the device surface was regulated by simultaneously changing the LED driving current and using neutral density filters placed between the LED and the phototransistor. The light intensity in the absence of neutral density filters was calibrated with a silicon photodiode (Hamamatsu S2387-33R). Care had been taken to prevent the scattered light other than attenuated LED light from impinging on the device during the light sensing measurement. Keithley sourcemeters 2400 and 2601 were used for all the transfer characteristic measurements. Another Keithley 2400 sourcemeter was used to provide the driving currents for the LED. All three sourcemeters were controlled remotely by a computer with a Labview program to ensure the synchronization between the electrical measurement and the LED lighting.

Spectral Photoresponse Measurement: Transfer curves were recorded while the phototransistors were shined with monochromatic light provided by a Xenon lamp coupled to a monochromator (Newport 74125). The intensity of the output light from the monochromator was in the range of μW cm^{-2}. The photoresponse was calculated by subtracting the $I_{ds(dark)}$ from the $I_{ds(light)}$ at a V_{gs} close to the turn-on voltage of the rightmost transfer curve and then normalizing with respect to the monochromatic light intensities.

Optical Absorption Measurement: For this measurement, a layer of PBDTTT:PCBM was spin-coated on a glass substrate with the same method described above. The optical absorption spectrum was recorded with a UV–visible spectrophotometer (Thermo Scientific, Evolution 201).

Supporting Information

Supporting Information is available from the Wiley Online Library or from the author.

Acknowledgements

The authors thank financial support by the Academic Research Initiative at the Domestic Nuclear Detection Office, the U.S. Department of Homeland Security under award 2014-DN-077-ARI069-03, and thank Arradiance Inc. for the growth of the HfO_2 layer with their benchtop ALD system (GEMStar-4 XT).

Received: July 26, 2016
Published online: November 29, 2016

[1] R. H. Hadfield, *Nat. Photonics* **2009**, *3*, 696.
[2] A. Armin, R. D. Jansen-van Vuuren, N. Kopidakis, P. L. Burn, P. Meredith, *Nat. Commun.* **2015**, *6*, 6343.
[3] P. L. Richards, C. R. McCreight, *Phys. Today* **2005**, *58*, 41.
[4] a) F. Li, C. Ma, H. Wang, W. J. Hu, W. L. Yu, A. D. Sheikh, T. Wu, *Nat. Commun.* **2015**, *6*, 8238; b) S. Park, S. J. Kim, J. H. Nam, G. Pitner, T. H. Lee, A. L. Ayzner, H. L. Wang, S. W. Fong, M. Vosgueritchian, Y. J. Park, M. L. Brongersma, Z. A. Bao, *Adv. Mater.* **2015**, *27*, 759; c) H. Yu, D. Kim, J. Lee, S. Baek, J. Lee, R. Singh, F. So, *Nat. Photonics* **2016**, *10*, 129; d) W. Dierckx, W. D. Oosterbaan, J. C. Bolsee, I. Cardinaletti, W. Maes, H. G. Boyen, J. D'Haen, M. Nesladek, J. Manca, *Nanotechnology* **2015**, *26*, 065201; e) W. M. Guo, Y. Liu, W. G. Huang, M. M. Payne, J. Anthony, H. E. Katz, *Org. Electron.* **2014**, *15*, 3061; f) M. Y. Lee, J. Hong, E. K. Lee, H. Yu, H. Kim, J. U. Lee, W. Lee, J. H. Oh, *Adv. Funct. Mater.* **2016**, *26*, 1445; g) R. M. Pinto, W. Gouveia, A. I. S. Neves, H. Alves, *Appl. Phys. Lett.* **2015**, *107*, 223301; h) Z. Qi, X. X. Liao, J. C. Zheng, C. A. Di, X. K. Gao, J. Z. Wang, *Appl. Phys. Lett.* **2013**, *103*, 053301; i) B. Yao, W. L. Lv, D. Q. Chen, G. Y. Fan, M. Q. Zhou, Y. Q. Peng, *Appl. Phys. Lett.* **2012**, *101*, 163301; j) H. Yu, Z. A. Bao, J. H. Oh, *Adv. Funct. Mater.* **2013**, *23*, 629; k) M. Zhu, S. C. Lv, Q. H. Wang, G. B. Zhang, H. B. Lu, L. Z. Qiu, *Nanoscale* **2016**, *8*, 7738.
[5] Z. Qi, J. M. Cao, H. Li, L. M. Ding, J. Z. Wang, *Adv. Funct. Mater.* **2015**, *25*, 3138.
[6] G. Y. Zhao, J. Liu, Q. Meng, D. Y. Ji, X. T. Zhang, Y. Zou, Y. G. Zhen, H. L. Dong, W. P. Hu, *Adv. Electron. Mater.* **2015**, *1*, 1500071.
[7] E. J. Gansen, M. A. Rowe, M. B. Greene, D. Rosenberg, T. E. Harvey, M. Y. Su, R. H. Hadfield, S. W. Nam, R. P. Mirin, *Nat. Photonics* **2007**, *1*, 585.
[8] J. Clark, G. Lanzani, *Nat. Photonics* **2010**, *4*, 438.
[9] M. H. Yoon, C. Kim, A. Facchetti, T. J. Marks, *J. Am. Chem. Soc.* **2006**, *128*, 12851.
[10] Y. Y. Hu, V. Pecunia, L. Jiang, C. A. Di, X. K. Gao, H. Sirringhaus, *Adv. Mater.* **2016**, *28*, 4713.
[11] H. Y. Chen, J. H. Hou, S. Q. Zhang, Y. Y. Liang, G. W. Yang, Y. Yang, L. P. Yu, Y. Wu, G. Li, *Nat. Photonics* **2009**, *3*, 649.
[12] D. M. Roessler, W. C. Walker, *J. Phys. Chem. Solids* **1967**, *28*, 1507.
[13] Y. B. Yuan, G. Giri, A. L. Ayzner, A. P. Zoombelt, S. C. B. Mannsfeld, J. H. Chen, D. Nordlund, M. F. Toney, J. S. Huang, Z. N. Bao, *Nat. Commun.* **2014**, *5*, 3005.
[14] Y. B. Yuan, J. S. Huang, *Adv. Opt. Mater.* **2016**, *4*, 264.
[15] F. Z. Wang, B. Zhang, Q. X. Li, Z. Z. Shi, L. Yu, H. Liu, Y. P. Wang, S. Y. Dai, Z. A. Tan, Y. F. Li, *J. Mater. Chem. A* **2016**, *4*, 1915.
[16] a) F. W. Guo, B. Yang, Y. B. Yuan, Z. G. Xiao, Q. F. Dong, Y. Bi, J. S. Huang, *Nat. Nanotechnol.* **2012**, *7*, 798; b) G. Konstantatos, M. Badioli, L. Gaudreau, J. Osmond, M. Bernechea, F. P. G. de Arquer, F. Gatti, F. H. L. Koppens, *Nat. Nanotechnol.* **2012**, *7*, 363.
[17] Y. L. Kim, H. Y. Jung, S. Park, B. Li, F. Z. Liu, J. Hao, Y. K. Kwon, Y. J. Jung, S. Kar, *Nat. Photonics* **2014**, *8*, 239.
[18] a) M. Aghamohammadi, R. Rodel, U. Zschieschang, C. Ocal, H. Boschker, R. T. Weitz, E. Barrena, H. Klauk, *ACS Appl. Mater. Interfaces* **2015**, *7*, 22775; b) E. J. Gansen, M. A. Rowe, M. B. Greene, D. Rosenberg, T. E. Harvey, M. Y. Su, R. H. Hadfield, S. W. Nam, R. P. Mirin, *IEEE J. Sel. Top. Quantum Electron.* **2007**, *13*, 967.